Climatology of Cyclone Size Characteristics and Their Changes during the Cyclone Life Cycle

IRINA RUDEVA AND SERGEY K. GULEV

P. P. Shirshov Institute of Oceanology, Moscow, Russia

(Manuscript received 10 January 2006, in final form 16 October 2006)

ABSTRACT

Climatology of the atmospheric cyclone sizes and their change over the cyclone life cycle is analyzed on the basis of tracking 57 yr of NCEP–NCAR reanalysis sea level pressure data over the Northern Hemisphere. To quantify the atmospheric cyclone sizes a coordinate transform was used, which allows for the collocation of the cyclone center with the virtual pole and for the establishment of a unique coordinate system for the further determination of cyclone geometry. This procedure was incorporated into a numerical cyclone tracking scheme and provided quantitative estimation of cyclone geometry at every stage of the cyclone development. Climatological features of the distribution of the cyclone size characteristics (effective radius, asymmetry) are considered for the cyclones with different central pressure, deepening rate, and lifetime. Mean effective cyclone radius may experience significant changes, ranging from 300–400 km over the continents to more than 900 km over the oceans. There is found to be a strong dependence of the cyclone effective radius on the cyclone lifetime and intensity, implying the largest cyclone sizes for the most intense and long-living transients. Analysis of size changes during the cyclone life cycle implies that the cyclone radius increases during the development stage from 50% to 150%. Size evolution during the cyclone life cycle implies a universal dependence of the normalized cyclone effective radius and the normalized cyclone age. The actual maximum cyclone radius can be determined from these two nondimensional parameters and cyclone central pressure. Further application of the analysis of cyclone size and shape are discussed.

1. Introduction

During recent years many studies have analyzed the climatology of cyclone activity using the outputs of the storm tracking in high resolution reanalysis and model data (e.g., Murray and Simmonds 1991; König et al. 1993; Sinclair 1997; Serreze et al. 1997; Blender et al. 1997; Sinclair and Watterson 1999; Sickmöller et al. 2000; Simmonds and Keay 2000a,b; Gulev et al. 2001; Hoskins and Hodges 2002, 2005; Hodges et al. 2003, and others). Despite the extensive analysis of different parameters of cyclone activity (e.g., cyclone frequencies), considerably less attention has been paid to the characteristics of the cyclone life cycle. These characteristics are very important for understanding the mechanisms of cyclone development, for the quantification of skills of numerical weather prediction (NWP) systems and for the detailed analysis of climate variability of cyclone activity. The number of cyclones may not necessarily vary drastically even in greenhouse gas experiments (e.g., Bengtsson et al. 2006); however, the characteristics of cyclone life cycle may undergo considerable changes. The works of Roebber (1984), Serreze (1995), Gulev et al. (2001), Zolina and Gulev (2002) analyzed cyclone deepening rates, cyclone intensity, lifetime, and propagation velocity. These are already a step forward compared with the quantification of exclusively cyclone numbers and frequencies.

Considering the parameters of the cyclone life cycle, of special interest is the cyclone size change. Humphreys (1927) first mentioned the change in cyclone size

Corresponding author address: Sergey Gulev, P. P. Shirshov Institute of Oceanology, RAS 36 Nakhimovsky Ave., 117851, Moscow, Russia.
E-mail: gul@sail.msk.ru

DOI: 10.1175/MWR3420.1

during its development in day and night. Nielsen and Dole (1992) analyzed cyclone sizes in National Meteorological Center [now the National Centers for Environmental Prediction (NCEP)] analyses, using the method of pressure deficit. Grotjahn et al. (1999) analyzed 12 Pacific cyclones, quantifying their sizes using wavelet transforms of the sea level pressure (SLP) field, and found that their radii roughly doubled during the first 4 days of development. For the same set, Grotjahn and Castello (2000) employed circular averaging of the perturbations of the geostrophic kinetic energy at 300 hPa for determination of cyclone size and found consistency with their earlier results (Grotjahn et al. 1999). Simmonds (2000) and Simmonds and Keay (2000a) provided comprehensive quantitative analysis of the cyclone sizes. Simmonds (2000) qualitatively supported the results of Grotjahn et al. (1999), although he found that cyclone sizes grow about 33% during the first 4-day period.

A complete quantitative characterization of the cyclone size is quite a difficult task in both methodological and physical senses. First, there is an uncertainty in the definition of the cyclone size. For instance, determination of the last closed isobar routinely used in synoptic meteorology largely depends on the isobar step and on the cyclone type. Second, even when a proper definition is established, there will still remain a number of methodological uncertainties in the direct estimation of the cyclone sizes, particularly associated with the interpolation. This justifies the use of the indirect estimates (Grotjahn and Castello 2000), based on the reasonably chosen ratios between spatial scales and atmospheric dynamic characteristics.

The aim of this work is to develop a methodology allowing for relatively accurate quantitative estimation of the cyclone sizes and to apply it for the analysis of changes in cyclone dimensions during the cyclone life cycle as revealed by 57 yr of the NCEP–National Center of Atmospheric Research (NCAR) reanalysis. In the following section we will describe the data and method of cyclone identification. In section 3, we outline the methodology of determination of cyclone dimensions. Section 4 presents the climatology of characteristics associated with the cyclone sizes. In section 5, we consider the size changes during the cyclone development. In the conclusion, section 6, we speculate about the prospects for the further application of our method.

2. Data and cyclone identification procedure

We used the NCEP–NCAR reanalysis data (Kalnay et al. 1996; Kistler et al. 2001) for the period from 1948 to 2004 in our study. The NCEP–NCAR reanalysis is a dynamically consistent dataset of basic atmospheric parameters, produced in an offline run of the T62 NCEP operational model. Although the data assimilation system in the NCEP model was frozen during the production time, the data assimilation input changed over time, especially starting from the late 1970s (epoch of satellite observations). This might create some artificial trends in the NCEP–NCAR reanalysis (e.g., White 2000), which are particularly pronounced in the poorly sampled Southern Hemisphere (Hines et al. 2000). Nevertheless, in the Northern Hemisphere the NCEP–NCAR 57-yr climatology is considered sufficient for the analysis of the natural climate variability during the last several decades. One can find a discussion of the role of different types of assimilated data in Bengtsson et al. (2004).

For the storm tracking of NCEP–NCAR data we used 6-hourly SLP output on a 2.5° × 2.5° grid. Storm tracking has been performed using a numerical tracking algorithm developed at the P. P. Shirshov Institute of Oceanology, Russian Academy of Science (IORAS). This algorithm is based on a reference dataset of storm tracks for the 42 winters of the period 1958–99 (Gulev et al. 2001), which was obtained using the semimanual software of Grigoriev et al. (2000). In the numerical method used the tracking is performed on a polar orthographic projection, which has 181 × 181 points with the center on the North Pole. This projection significantly enlarges polar and midlatitude regions in comparison to the Tropics, allowing for more effective cyclone identification and tracking. Interpolation of the original 2.5° × 2.5° data onto the polar orthographic 181 × 181 grid was carried out using the modified method of local procedures (Akima 1970). This method is very accurate and does not create any intermediate artificial extrema.

The preprocessing of the SLP data includes the dynamical interpolation of the 6-hourly SLP fields onto shorter time steps (1-hourly). This involves the numerical solution of $\partial(\mathrm{SLP})/\partial t = \mathbf{u} \cdot \nabla(\mathrm{SLP})$, where $\mathbf{u}$ is the cyclone propagation vector (because the time derivative and the gradient are known $\mathbf{u}$ can be obtained). Thus, SLP patterns are allowed to propagate, which is not necessarily the case for purely linear interpolation schemes. The returned SLP fields at a higher temporal resolution allow for the effective separation of the cyclone migrations from the distances between the centers of the neighboring cyclones. Interpolation as an initial step of tracking does not involve yet the consideration of individual cyclones and provides only the SLP patterns on a higher temporal resolution. The identification of cyclones is based on the analysis of the

local SLP minima. This step involves several iterations and includes the analysis of SLP derivations computed from the 17 neighboring points, determination the so-called impact area in which the analysis of SLP characteristics was further performed to locate the cyclone center. The tracking procedure itself starts from the method of the closest neighbors, also employed as an initial step in the schemes of Murray and Simmonds (1991), König et al. (1993), Sinclair (1997), Hodges (1994), Hoskins and Hodges (2002), and others. This step provides a first guess of cyclone migration. Further identification of the tracks involves the three-pass analysis of cyclone propagation velocities, sorting of the crossing trajectories and separate analysis of the stationary cyclones. Recently, the skills of the numerical tracking scheme were considerably improved using several years output of the atmospheric GCM with original temporal resolution of 1 h provided by European Centre for Medium-Range Weather Forecasts (ECMWF; Jung et al. 2006). Validation of the tracking scheme against the results of semimanual tracking of Gulev et al. (2001) showed very close comparability with this reference dataset. This scheme was used for the identification of cyclones in reanalysis products (Zolina and Gulev 2003), climate models Loeptien et al. (2006, manuscript submitted to *Climate Dyn.*), and an ECMWF high-resolution AGCM (Jung et al. 2006).

Alternative cyclone tracking algorithms (e.g., Sinclair 1994, 1997) strongly recommend using vorticity for the cyclone identification and tracking. Similarly the scheme of Murray and Simmonds (1991) and Simmonds and Murray (1999) analysed the Laplacian maximum in the vicinity of an SLP minimum for the identification of cyclones. Hodges (1994, 1999) as well as Hoskins and Hodges (2002) and Hodges et al. (2003), employ the vorticity at 850 hPa arguing that vorticity focuses on the small-spatial-scale end of the synoptic range and, thus, allows for identification of smaller-scale systems. Gulev et al. (2002), using band-pass statistics of geopotential heights, demonstrated very different locations of the maximum intensities of large- and small-scale synoptic features. The use of lower-level vorticity implies a less restrictive (Sinclair 1997) definition of a cyclone than that purely based on synoptic consideration of SLP. Furthermore, it requires the application of the smoothing procedures and makes the results dependent on the smoothing parameters as demonstrated by Sinclair (1997). Sea level pressure is used for the tracking in many studies of cyclone intensity (Blender et al. 1997; Sickmöller et al. 2000; Serreze et al. 1997; Geng and Sugi 2001; Trigo 2006; Bauer and Del Genio 2006). Similarly, many works are based on the vorticity feature tracking (Sinclair 1997; Simmonds and Keay 2000a,b; Hoskins and Hodges 2002, 2005; Hodges et al. 2003). One can find discussions on the proper choice of the measure for cyclone identification and tracking in Hodges et al. 2003, Jung et al. 2006, and Bauer and Del Genio 2006. In section 6 we will show some comparisons of the cyclone size estimates derived from different tracking algorithms.

The output of the tracking (coordinates, time, and corresponding SLP values in the cyclone centers) can be further used for characterization of cyclone activity. Spatial distribution of cyclone activity can be characterized by cyclone numbers (the number of SLP minima passing through a box during a given time interval, with multiple entries being ignored) and cyclone frequencies (the number of the pressure minimum events, counted by an Eulerian observer within the box during the chosen time interval), whose spatial mapping was performed on a grid, which has $5° \times 5°$ grid cells south of 70°N and variable grid cell sizes (from $10° \times 5°$ to $15° \times 8°$) north of 70°N, including the circular cell centered at the North Pole and implied by a circle rounded at 88°N (Zolina and Gulev 2002). Characteristics of the cyclone life cycle include the cyclone minimum central pressure and cyclone lifetime, computed from the number of 6-hourly intervals forming the cyclone trajectory. Note that the accuracy of the lifetime estimation is approximately equal to $\pm k/2$ hours, where k is the time resolution (6 h in our study) of the reanalysis (Gulev et al. 2001). In the present study only cyclones living longer than 18 h are considered.

Deepening rates were computed from adjacent 6-hourly cyclone central pressure values using forward time differencing. The mean and maximum deepening rates, δSLP and $\delta\text{SLP}_{\text{max}}$, respectively, were computed as the average over deepening rates (computed for 6-hourly time steps) during the cyclone deepening and as the maximum deepening rate during the cyclone lifetime, respectively. Following Roebber (1984, 1989) and Serreze (1995) all deepening/filling rates were normalized as $\langle\delta\text{SLP}\rangle = \delta\text{SLP}\ (\sin\phi_{\text{ref}}/\sin\phi)$, where ϕ_{ref} is a reference latitude, taken in this study as 45°. This normalization accounts for a latitudinal dependence of planetary vorticity. The definition of deepening rate applied in our study follows the works of Sanders and Gyakum (1980), Roebber (1984), Serreze (1995), and others. This is different from the definition suggested by Lim and Simmonds (2002) who considered the relative central pressure changes that account for the potential impact of background pressure gradients on the estimates. However, under that method, the deepening of the central cyclone pressure may not necessarily imply the intensification of cyclones. Cyclone propagation velocities were estimated from the trajectories using

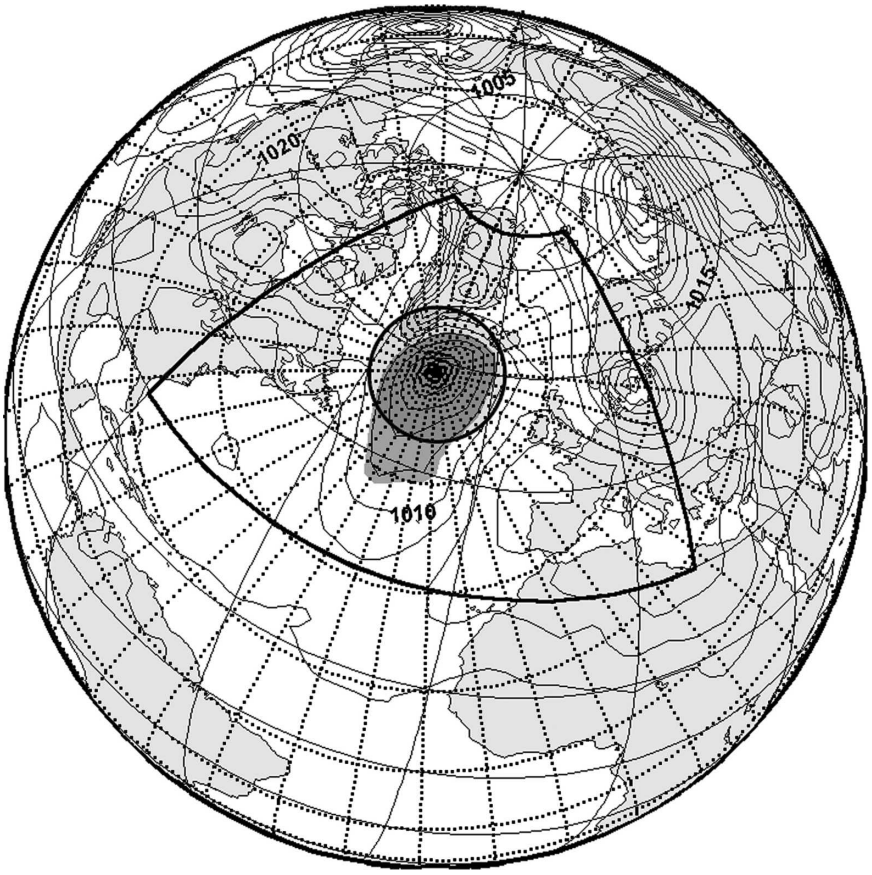

FIG. 1. Collocation of the virtual pole with the center of the cyclone at 0000 UTC 23 Nov 2004. Boldface coordinate lines correspond to the original coordinate system and dotted lines to the new coordinate system, collocated with the cyclone center. Gray areas mark the determined cyclone area. The boldface circumference corresponds to the equivalent circle whose radius is considered as cyclone effective radius.

simple numerical procedures. The cyclone mean velocity was estimated as the mean of individual velocities during cyclone lifetime. These characteristics provide a standard set of parameters which were used along with the cyclone size characteristics.

3. Estimation of cyclone size characteristics

To determine the characteristics of cyclone geometry we applied a transformation of the coordinate system by the collocation of the cyclone center with the center of the polar coordinate system. This approach is frequently used in ocean general circulation and ice modeling and implies the shift of the poles from their original locations in order to achieve a better spatial resolution in high latitudes and to avoid the computational uncertainties in the areas of the strong meridian convergence. In our work, this transformation provides a computational convenience for the further interpolation and estimation of the cyclone dimensions. For every step of the cyclone tracking the coordinate transform established a coordinate system with a virtual pole in the cyclone center and the 36 radii forming an azimuthal grid on which SLP fields were interpolated by the method of local procedures (Akima 1970), as in the case with interpolation onto the polar orthographic grid. Figure 1 shows an example of the application of the procedure to one cyclone in the North Atlantic at 0000 UTC 23 November 2004, demonstrating the collocation of the azimuthal grid with the actual cyclone. This approach allowed us to establish a firm ground for the further quantification of the cyclone geometry characteristics.

The definition of cyclone size is not a trivial process. Any choice of the measure will suffer from the uncertainties of determining the area belonging to the cyclone. Simmonds (2000) argues "... there is no single, 'best' definition of radius or size of a system ..." For instance, the threshold on the minimum radial SLP gradient may strongly vary in different cyclone sec-

tions, being typically larger in the back section of cyclones in comparison to the forward area. Alternatively, a threshold on the pressure deficit for a particular cyclone will be very much dependent on the cyclone intensity and the background field pressure. According to the analysis of Gulev et al. (2001) the central pressure in the reanalysis can vary from 1010–1020 to 950–960 hPa, implying the variations in pressure deficits from 10 to about 50 hPa.

Following Simmonds and Keay (2000a) and Simmonds (2000) we estimated the cyclone size by searching along 36 radii (with 10° angular step) for the location where the first radial derivative of SLP computed at radial spatial steps of 100 km, falls to zero:

$$\frac{\partial \mathrm{SLP}}{\partial r} = 0. \quad (1)$$

In this location we determined the "critical" SLP value for a given radius. If within 1500 km the condition of (1) was not satisfied, the first guess radius for this direction was set to 1500 km with the SLP in this location set to the critical value. Given the relatively coarse resolution of the NCEP–NCAR reanalysis, we required the minimum radius to be 200 km. Then the minimum among all 36 critical SLP values was considered as the so-called "last closed isobar" for the particular cyclone. The locations of this isobar at every radius then can be determined by a simple interpolation. This location returns the actual azimuthal dimension of cyclone for a given radius r_i. Finally, 36 locations mark the geometry of the cyclone for a given time step. This geometry is characterized by the curve M, capturing the area S_M that could be determined through the triangle summation:

$$S_M = \sum_{i=1}^{36} s_i, \quad (2)$$

where s_i is the individual area of the triangles forming the cyclone. Then the area obtained in units L^2 was attributed to the virtual circumference, whose virtual radius was defined as the cyclone effective radius for this time step:

$$r_{\mathrm{ef}} = [(S_M/\pi)^{1/2}]. \quad (3)$$

This effective radius gives an effective measure of the cyclone size. Figure 1 shows for 0000 UTC 23 November 2004 the actual cyclone shape and the equivalent circle, returning the effective radius. Additionally, we determined the cyclone asymmetry by finding the largest diameter among the 18 available and searching for the smallest diameter within ±20° of the diameter orthogonal to the largest. Thus, we determined the major and the minor cyclone radii whose ratio further quantified the cyclone asymmetry.

The virtual coordinate system was also used for the computation of the routine local dynamical characteristics of the SLP field, such as the Laplacian and geostrophic vorticity. These were estimated for every time step. The described procedure allowed for the determination for every time moment of the cyclone life cycle of many characteristics of the cyclone geometry (cyclone area, effective radius, the large and the small cyclone radii) as well as the Laplacian and vorticity. The methodology applied in our study is very similar to the approach used by Simmonds and Keay (2000a) and Simmonds (2000). They used a different scheme for cyclone tracking (Murray and Simmonds 1991; Simmonds and Murray 1999), which takes into account the Laplacian maximum in the vicinity of SLP minimum for a proper identification of cyclone center. Furthermore, their procedure searches outward along some azimuthal lines for the locations where the Laplacian becomes negative. These locations define the cyclone area and then the so-called notional radius is determined assuming this area to be a circle. Sinclair (1997) used similar procedure for the determination of cyclone domains, although his methodology has some differences from applied here and in Simmonds and Keay (2000a). One can find detailed discussion on this point in Simmonds and Keay (2000a).

4. Climatology of cyclone size characteristics

To characterize climatological features of the cyclone size characteristics, we show winter (January–March; JFM) and summer (July–September; JAS) climatologies of the number of cyclones (Fig. 2a,b). This choice of seasons (JFM and JAS) allows for comparison with earlier results of Gulev et al. (2001) and Zolina and Gulev (2002) based on the same data. Cyclone numbers are presented as cyclone counts per unit area of 218 000 km^2 (5° × 5° cell at 45°N) per season as in Gulev et al. (2001) and Zolina and Gulev (2002). General climatological characteristics of cyclone activity over the Northern Hemisphere in the NCEP–NCAR reanalysis for the period from 1948 to 2004 are not significantly different from earlier estimates based on the same SLP product (e.g., Gulev et al. 2001). In winter they effectively mark the Atlantic and Pacific storm tracks where the number of cyclones varies from 5 to 10 events per season, being up to 2.5 times higher than that over the continents. Summer distribution shows higher cyclone counts over the continents, where the number of events may be 1.5 to 4 times higher than over the oceans. Maxima of the number of deep (<980 hPa) cyclones (Figs. 2c,d) are primarily associated with the oceanic storm tracks, demonstrating a considerably larger num-

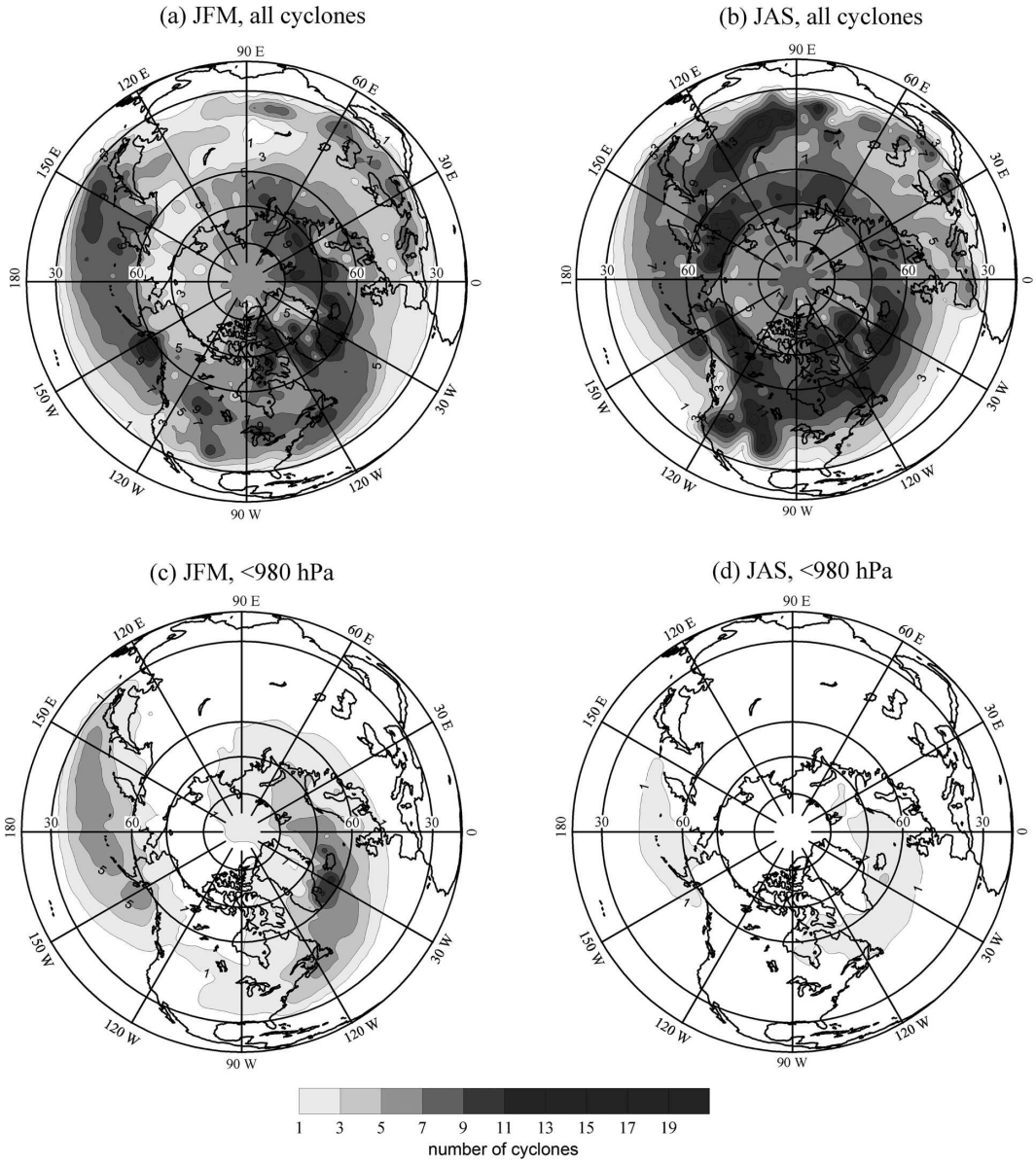

FIG. 2. (a) Winter and (b) summer distribution of the total climatological number of cyclones along with the (c) winter and (d) summer distributions of the number of deep (<980 hPa) cyclones over the Northern Hemisphere. Cyclone numbers are given per 218 000 km^2 per season.

ber of deep cyclones in winter than in summer. Thus, in winter the largest number of deep cyclones varies from 5–6 in the North Pacific to 10–12 in the North Atlantic, being in summer about 1.5–2 and 3–4 in the Pacific and Atlantic, respectively.

Now we turn to the analysis of cyclone size characteristics. Figure 3 shows the winter and summer climatology of the cyclone effective radius. Being derived from the sizes of cyclones passing particular grid cells, these maps represent a joint effect of the size changes between different regions and size evolution during the cyclone life cycle. Cyclone sizes over the oceans are larger than those over the continents for both seasons with differences being statistically significant for most areas. Over the midlatitudinal oceanic storm tracks the effective cyclone radius is typically higher than 600 km, implying cyclone areas of about 1.2×10^6 km^2 and larger. Over the continents the effective cyclone radius primarily varies from 300 to 600 km. The smallest cyclones with effective radii of less than 400 km occur in the subpolar and subtropical regions as well as over the Rocky Mountains. Given that the tracking is based on

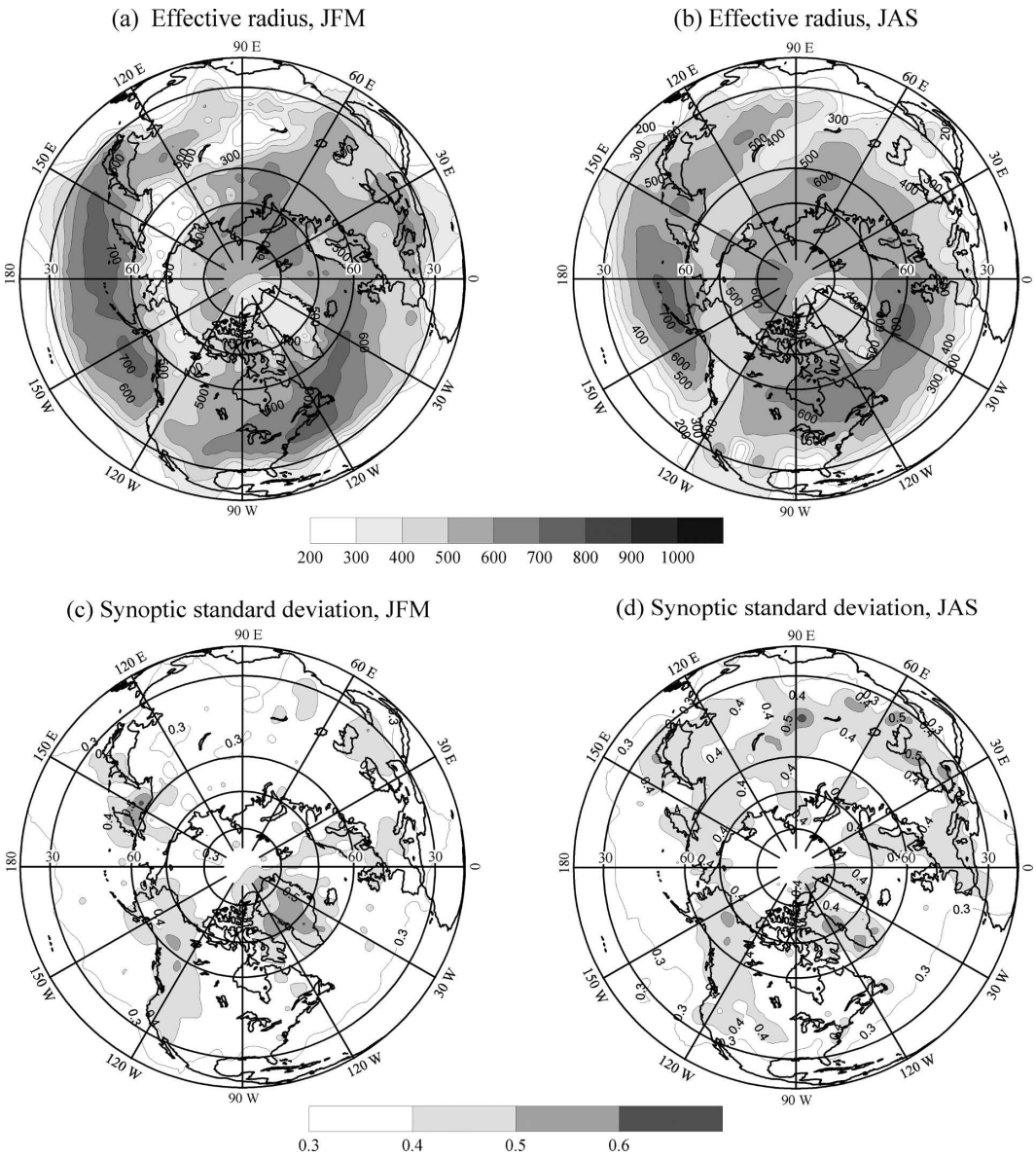

FIG. 3. (a) Winter and (b) summer climatological distribution of the cyclone effective radius (km) as well as (c) winter and (d) summer synoptic standard deviations of the cyclone effective radius, scaled with climatological means. Contour interval is 100 km for the cyclone radius and 0.1 for normalized standard deviations.

reduced SLP, note that estimates over mountainous regions in our study may be less accurate than those over areas near sea level, and should therefore be considered with care. During summer, cyclone size estimates for the same locations as in winter are typically smaller by 20%–40% (Fig. 3b). These changes are associated with both changes in the cyclone life cycle and changes in the locations of trajectories during the year. Compared to Simmonds and Keay (2002) results derived from the NCEP–NCAR reanalysis for 1958–97, our spatial distributions are quite similar for both winter and summer seasons; however, the cyclone radii have somewhat larger absolute values. Figures 3c,d show standard deviations of the cyclone effective radii for the two seasons, scaled with seasonal means. They were computed from the standard deviations of the effective radii of individual cyclones during each season and thus reflect the magnitude of synoptic variability of the cyclone effective radius. Normalized standard deviations of the cyclone effective radius generally vary from 0.3 to 0.7, showing the smallest values over the oceanic storm tracks (0.25–0.4) and the largest values over the

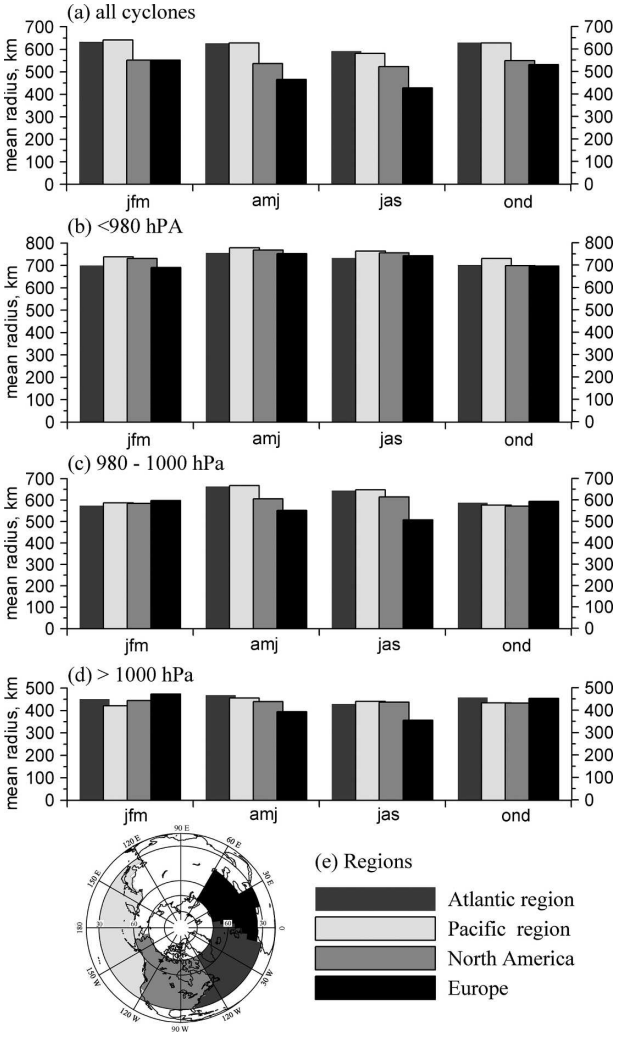

FIG. 4. Averaged estimates of the cyclone effective radius over different regions for (a) all cyclones, (b) deep (<980 hPa), (c) moderate (980–1000 hPa), and (d) weak (>1000 hPa) cyclones. (e) The map shows the subdivision of the regions.

continental storm tracks (0.5–0.65) for both winter and summer seasons. This implies that over the oceanic storm tracks synoptic variability of the cyclone size is considerably smaller than over the continents.

Figure 4 shows seasonal estimates of the effective cyclone radius of the cyclones of different intensities over the two oceanic basins (North Atlantic and North Pacific) and the two continental domains (North America and Europe). The regions selected are shown in Fig. 4e. The cyclone has been attributed to the selected region if its minimum central pressure was observed over that region. This figure reflects the joint effect of the distribution of cyclones of different intensity over the Northern Hemisphere and regional changes in the cyclone size. Seasonal changes are hardly detectable in the sizes averaged over all cyclones (Fig. 4a) and for cyclones of different intensities (Figs. 4b–d). Thus, that seasonal march in cyclone radius is primarily driven by the annual cycle of the number of cyclones of different intensities over both oceans and continents. Effective radii of the intense cyclones (<980 hPa) range from 650 to 780 km, being approximately 15%–20% higher than for the moderate cyclones (980–1000 hPa) and more than 50% larger than for the shallow cyclones (>1000 hPa).

Figures 5a,b shows the occurrence histograms of cyclone effective radii averaged over the cyclone life cycle. During both winter and summer the modal value of the cyclone effective radius is 20%–30% larger over the oceans in comparison to the continents. Moreover, the oceanic probability density distributions (PDFs) demonstrate a considerably higher occurrence frequency for radii exceeding 600 km, while the continental PDFs show higher probability for the smaller radii. Thus, in summer about 25% of oceanic cyclones demonstrate the mean effective radius exceeding 650 km, while over the continents the number of these cyclones was smaller than 14%. The corresponding estimates for winter are 33% and 19%. The continental histograms of the maximum effective radius during the cyclone life cycle (Figs. 5c,d) are somewhat more peaked. About 38% of winter cyclones developing over the ocean have a maximum effective radius larger than 900 km (cyclone areas 2.5×10^6 km^2). At the same time, the percentage of the continental cyclones with the maximum radius larger than 900 km is 22%. Although less pronounced, this tendency is also evident during summer. The distribution of the effective radius for the period of maximum cyclone intensity (Figs. 5e,f) shows qualitatively the same features as for the maximum cyclone effective radius for both winter and summer.

Figure 6 shows occurrence histograms of the mean cyclone effective radius for different characteristics of the cyclone life cycle. Effective cyclone radius increases with the decreasing central pressure (Figs. 6a,b). For the cyclones deeper than 980 hPa the modal value of the effective radius varies from 700 to 800 km, from 500 to 600 km for the moderate cyclones (980–1000 hPa), and from 350 to 500 km for the shallow cyclones (>1000 hPa) for both winter and summer. The longest-living cyclones (>5 days) are characterized by the largest effective radius in comparison to the cyclones with shorter lifetimes (Figs. 6c,d). About 20% (less than 10%) of cyclones with a lifetime of longer than 5 days during winter (summer) have a mean effective radius larger than 800 km. The smallest sizes (with modal values of the effective radius from 300 to 400 km in winter and 200 to 300 km in summer) are observed for cy-

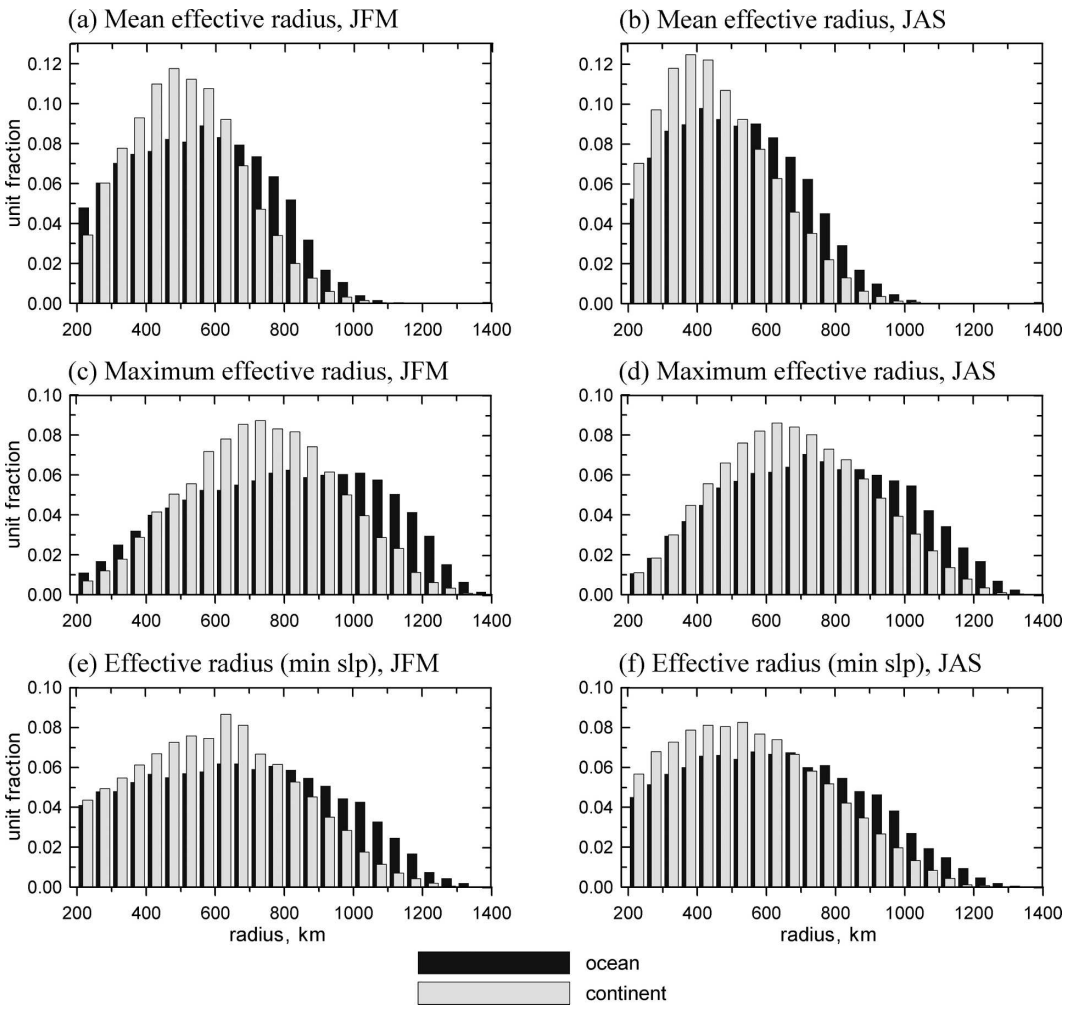

FIG. 5. Occurrence histograms of the cyclone effective radius computed for oceanic (black) and continental (light gray) cyclones for (a), (c), (e) winter and (b), (d), (f) summer. (a), (b) Histograms for the mean values of radius, (c), (d) histograms for the maximum radius, (e), (f) histograms for the radius at the moment of minimum cyclone central pressure.

clones with lifetimes shorter than 2 days. Cyclones with larger deepening rates are characterized by larger effective radii compared with slowly deepening transients (Figs. 6e,f). This is especially pronounced during the winter season when more than 34% of cyclones with a deepening rate of $\langle \delta \mathrm{SLP} \rangle > 4$ hPa (6 h)$^{-1}$ exhibit a mean effective radius larger than 700 km. Separate analysis for maximum deepening rates $\langle \delta \mathrm{SLP} \rangle_{\max}$ (not shown) shows that the largest effective radii of about 1000–1200 km occur for rapidly deepening cyclones with a deepening rate $\langle \delta \mathrm{SLP} \rangle_{\max}$ exceeding 1 Bergeron [24 hPa (24 h)$^{-1}$; Sanders and Gyakum 1980; Rogers and Bosart 1986].

Our methodology allows for the determination of the large and small cyclone radii, and makes it possible to quantify the shape of the cyclones. We computed the ratio between the smallest ($D_{\min}$) and the largest ($D_{\max}$) diameters for each cyclone. Figure 7 shows winter and summer distributions of the ratio $\eta = D_{\min}/D_{\max}$, quantifying cyclone asymmetry. The largest values of η are observed over the oceanic storm tracks where they are typically higher than 0.5. The smallest values of η (less than 0.3–0.4) are observed over the continental areas, where cyclones are most asymmetric. The greater asymmetry of continental cyclones compared to oceanic ones may be explained by the heterogeneous surface forcing coming from orography, land cover, water bodies, and so on. Synoptic standard deviations (Figs. 7b,d) vary for most areas from 0.15 to 0.30, showing the largest synoptic variability of η over the continents and somewhat weaker variations over the oceans. Figure 8 shows occurrence histograms of the ratio η for winter

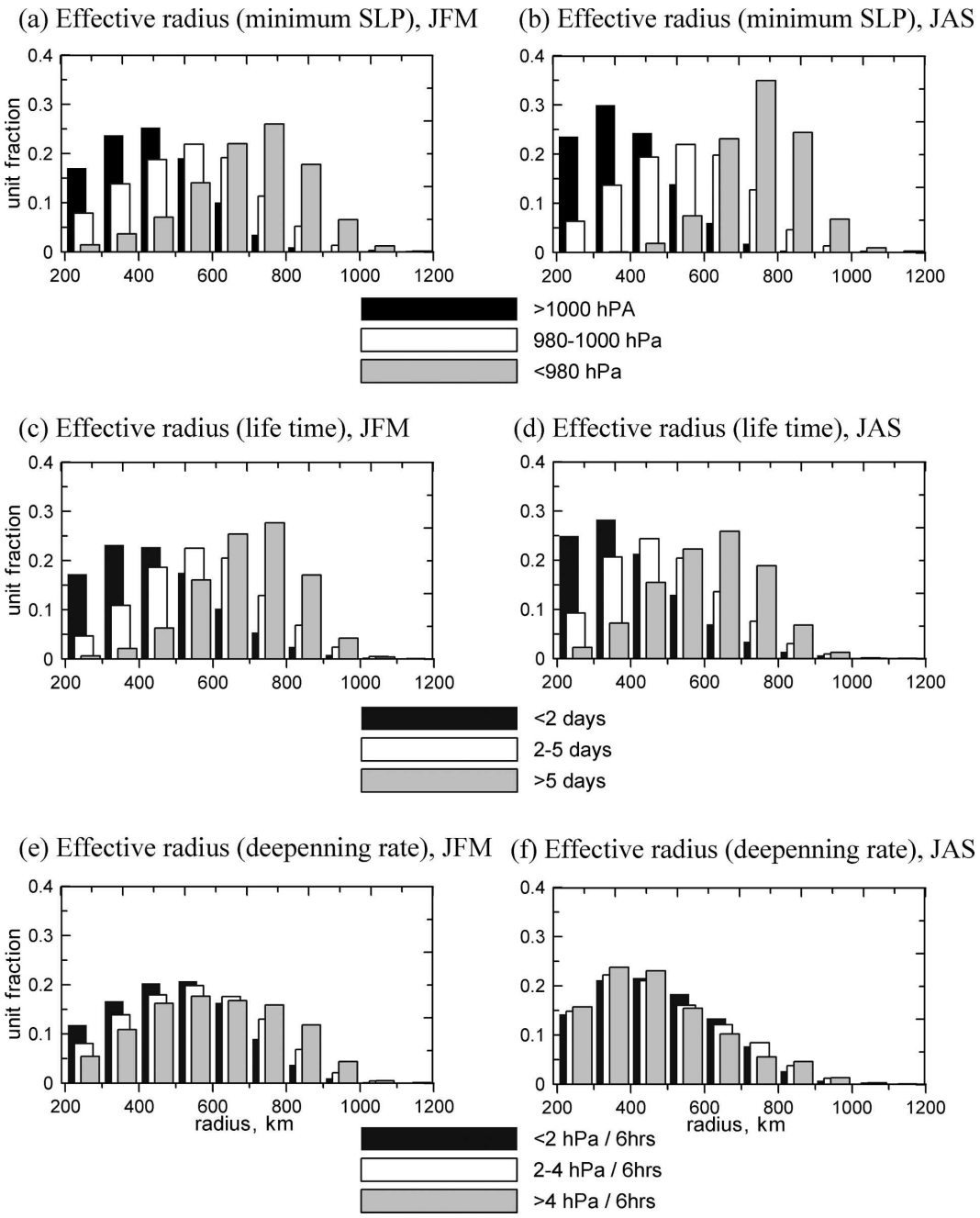

FIG. 6. Occurrence histograms of the cyclone effective radius computed for (a), (c), (e) winter and (b), (d), (f) summer for the cyclones with different (a), (b) minimum central pressure, (c), (d) lifetime, and (e), (f) deepening rate.

and summer, implying higher η values in winter than in summer. About 70% of cyclones during winter and 65% in summer are characterized by $0.3 < \eta < 0.7$. About 3% of cyclones in winter and nearly 2% of summer cyclones are characterized by η values exceeding 0.8, implying nearly circular cyclones. These cyclones are typically observed over the midlatitude oceanic storm tracks. The smallest ratios of less than 0.2 are observed for 10% of winter cyclones and more than 13% of summer cyclones. They primarily occur over the continental mountain areas. Again, these estimates should be taken with caution, as they can be potentially affected by the pressure reduction to sea level in the reanalysis data.

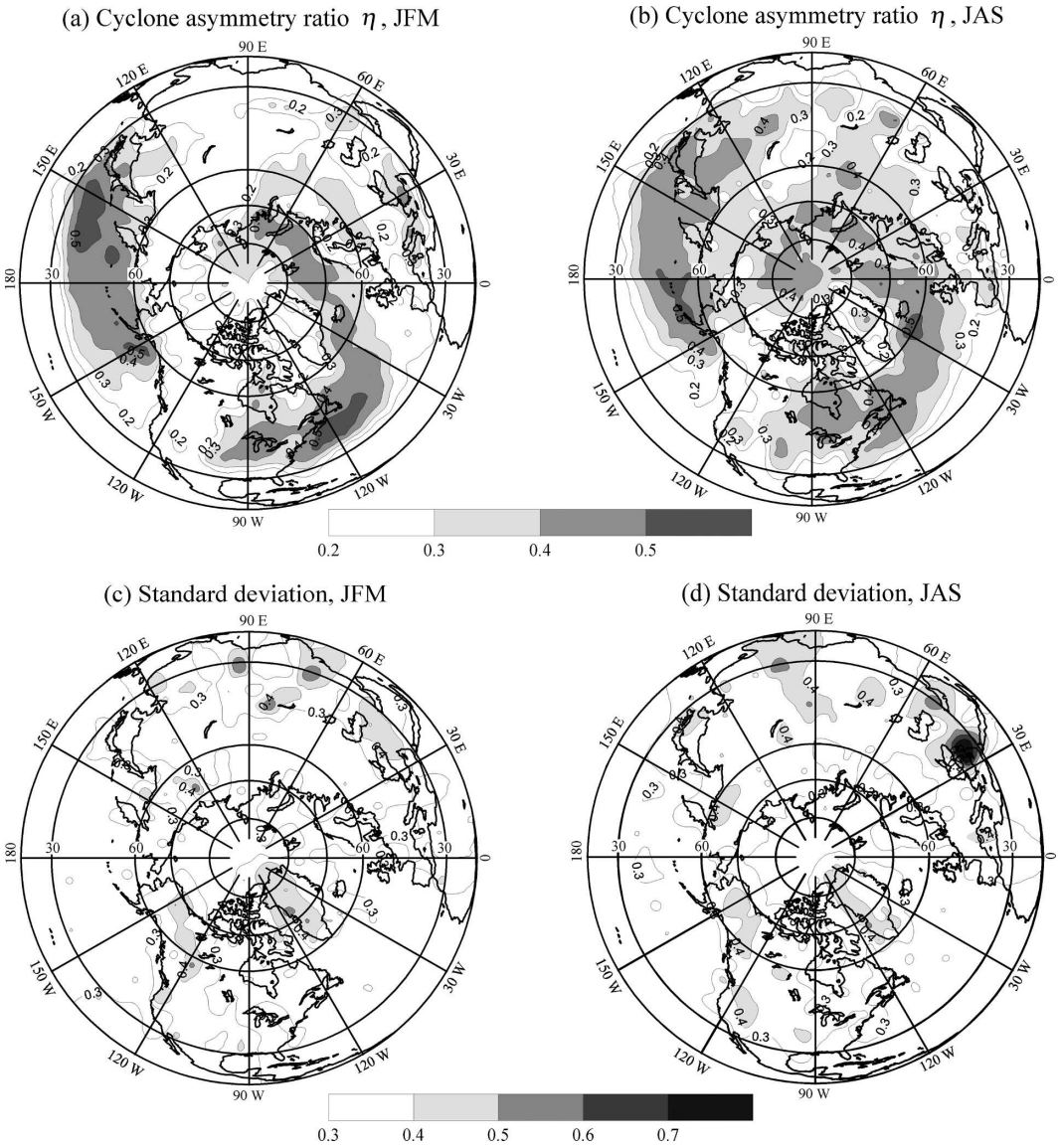

FIG. 7. (a) Winter and (b) summer climatology of the ratio η, defining the cyclone asymmetry along with the (c) winter and (d) summer synoptic standard deviations of the ratio η over the Northern Hemisphere, scaled with climatological means. Contour interval is 0.1.

5. Cyclone size and shape changes during the life cycle

Simmonds (2000) has shown that cyclone size increases by about 33% during the first 4 days of the development of the long-living cyclones. Figures 5 and 6 also imply that cyclone sizes may change during the cyclone life cycle. Because of the strong variability of the cyclone lifetime, comparison of cyclone size for different stages of the cyclone life cycle is quite difficult. Simmonds (2000) demonstrated (see his Fig. 3) some similarity of the cyclone size change for cyclones with different lifetimes. To analyze the cyclone size evolution during different stages of development, we introduced a nondimensional cyclone lifetime that normalizes the cyclone age by the actual lifetime:

$$\tau(t) = \frac{t}{T}, \tag{4}$$

where $\tau(t)$ is the normalized cyclone age in the time moment t of the cyclone's life cycle and T is cyclone lifetime. The normalized cyclone age varies from 0 to 1 for all cyclones and allows for the effective comparison

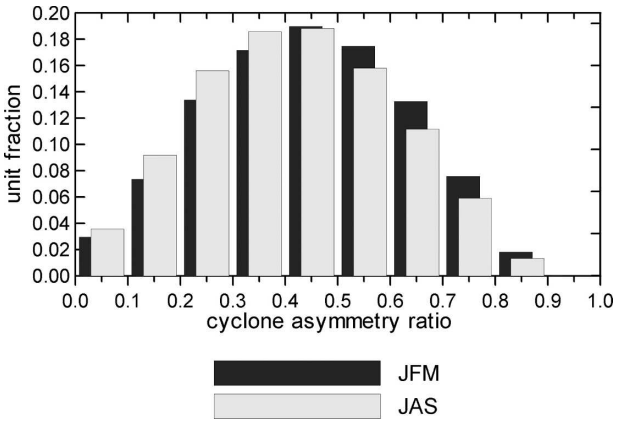

FIG. 8. Winter (black) and summer (white) occurrence histograms of the ratio η, defining the cyclone asymmetry.

of cyclone characteristics during the life cycle. To quantify cyclone size changes during the life cycle we applied spline interpolation to the cyclone effective radius that provided estimates of cyclone radius at 0.02 unit intervals of the nondimensional lifetime (51 points for the life cycle of every cyclone).

Figure 9a shows the evolution of the PDF of the cyclone effective radius during the normalized cyclone life cycle for the winter season. Right after cyclone generation the distribution of the cyclone effective radius is very asymmetric, with modal values of 200–300 km (20% of transients) and many cyclones whose radii range from 300 to 700 km. The increase of the cyclone effective radius occurs from this time moment to τ = 0.45–0.55, when the cyclone effective radius reaches the modal values of 500–600 km. During the cyclone decay stage the modal value of the cyclone effective radius decreases to 200–250 km and the distribution of radii again becomes strongly asymmetric. Summer evolution of the probability density distribution of the cyclone effective radius (Fig. 9b) is characterized by smaller maximum modal values (about 450 km), a more peaked distribution and more stable values of cyclone effective radius during the mature stage of cyclone development (τ = 0.2–0.8). Figure 9 implies that the distribution of the cyclone radius is more symmetric at the stage of maximum cyclone development than at the stages of cyclone generation and decay, especially in winter. Thus, for the stages of cyclone generation and decay the mean effective radius analyzed by Simmonds (2000) is typically 20%–30% larger than the modal radius. The differences between the modal and mean values become considerably smaller for the stage of the maximum cyclone intensity.

Our estimates of the growth of the cyclone radius with the cyclone age are in qualitative agreement with Simmonds (2000) who performed the averaging of cyclone radii for different bins of the cyclone lifetime. Similar analysis of our data for daily bins of the cyclone lifetime (Figs. 10a,b) clearly shows that the cyclone effective radius increases with increasing lifetime. However, Figs. 10a,b imply similarity of the cyclone size behavior during cyclone development for quite wide

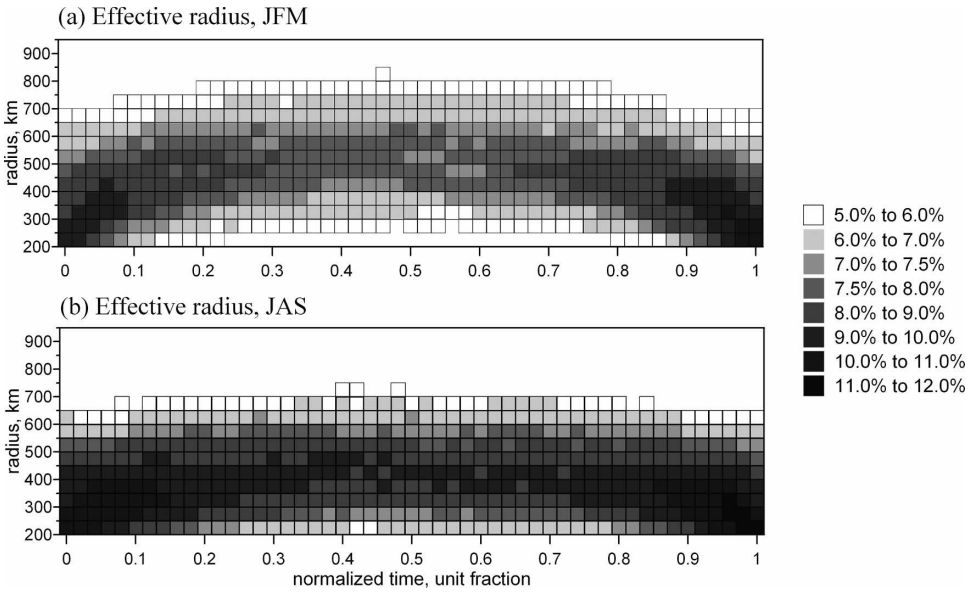

FIG. 9. (a) Winter and (b) summer evolution of the PDF of cyclone effective radius (km) during the nondimensional cyclone lifetime.

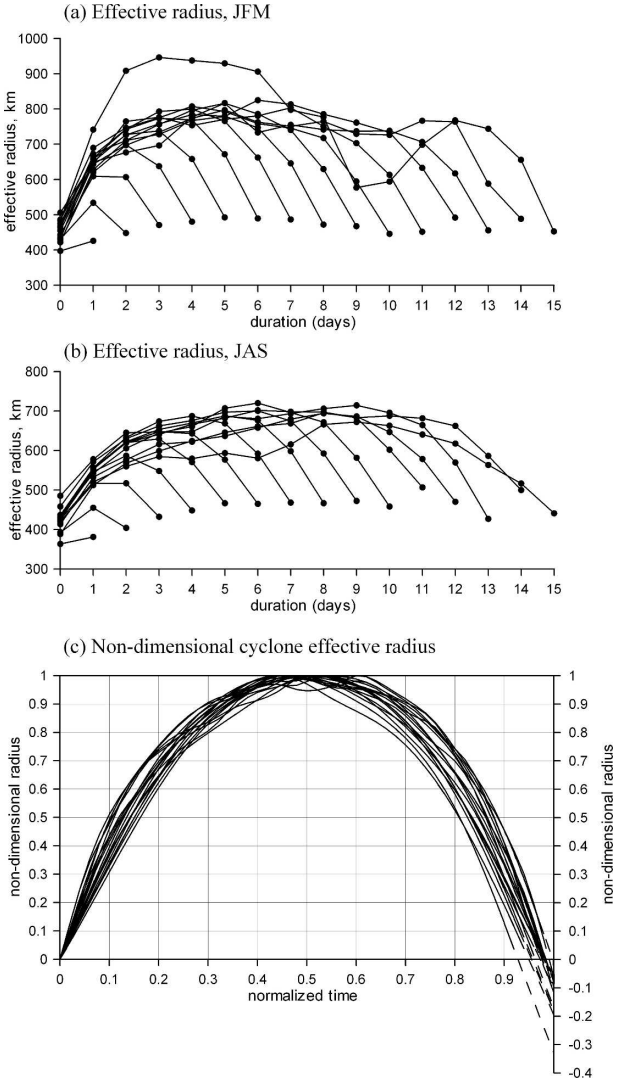

FIG. 10. (a) Winter and (b) summer changes of the cyclone effective radius, averaged for daily bins and changes of the nondimensional cyclone effective radius with nondimensional cyclone age for (c) different cyclone lifetimes.

range of lifetimes. To quantify this similarity, in addition to (4) we introduced a nondimensional cyclone effective radius ρ:

$$\rho(t) = \frac{R(t) - R_0}{R_{\max} - R_0}, \tag{5}$$

where $R(t)$ is the cyclone radius at the time moment t, $R_{\max}$ is the maximum effective radius during the cyclone life cycle, R_0 is assigned to the radius in the beginning of the life cycle. The values of ρ in a general case vary from 0 to 1. In Fig. 10c we show the dependencies of the nondimensional cyclone effective radius on the nondimensional cyclone age. Dependencies from Figs. 10a,b after the normalization form the family of curves shown in Fig. 10c, which are quite close to each other. The largest effective radius is typically achieved at the time moment $\tau_{\max} = 0.45$–0.55. The normalization eliminates the dependency of $\tau_{\max}$ on the cyclone lifetimes while the absolute values of maximum cyclone radii were clearly dependent on the actual lifetime (Figs. 10a,b). Thus, normalization (4), (5) introduces two nondimensional parameters that can be used to parameterize the cyclone size change during the life cycle.

Figure 10c implies the possibility to parameterize the change of the nondimensional cyclone effective radius ρ during the nondimensional cyclone lifetime τ. For this purpose we considered the dependence

$$\rho(\tau) = 1 - \left(\frac{|\tau - \tau_{\max}|}{\tau_{\max}}\right)^{\gamma}, \tag{6}$$

where $\tau_{\max}$ is the normalized time at which the maximum effective radius is observed and γ is the shape parameter. According to (6), clearly ρ goes to zero at $\tau = 0$ and $\rho = 1$ at $\tau = \tau_{\max}$. Cyclones of different intensities still may imply some variability in the behavior of the normalized cyclone size on the nondimensional lifetime (Fig. 10c). This variability can be accounted for by the dependency of γ and $\tau_{\max}$ in (6) on the cyclone minimum central pressure. For the cyclones with the minimum central pressure less than 1013 hPa

$$\gamma = \xi_0 + \xi_1 \times (1013 - \mathrm{SLP}_{\min})$$
$$\tau_{\max} = \zeta_0 + \zeta_1 \times (1013 - \mathrm{SLP}_{\min}), \tag{7}$$

where $\mathrm{SLP}_{\min}$ is the cyclone minimum central pressure (hPa), ξ_0, ζ_0, ξ_1, and ζ_1 are empirical coefficients of which ξ_0 and ζ_0 are nondimensional and ξ_1 and ζ_1 have the dimension of $(\mathrm{hPa})^{-1}$. Estimation of the coefficients by least squares implied quantitative values $\xi_0 = 2.179$, $\zeta_0 = 0.375$, $\xi_1 = -0.0133\ \mathrm{hPa}^{-1}$, $\zeta_1 = 0.0064\ \mathrm{hPa}^{-1}$. Parameterization (6)–(7) is valid for the actual time moments $t_0 + 6$ h, t_0 being the time of cyclone generation, and for the cyclone lifetimes less than 7 days (92% of all cyclones identified). For the remaining 8% of cyclones with the lifetimes longer than 7 days the central pressure exhibits intermediate extrema associated with the cyclone regeneration. Note that Simmonds (2000) has also demonstrated complicated behavior of the cyclone radius for the long-lived cyclones. Estimates of the accuracy of approximation (6)–(7) show that the approximation uncertainties (quantified as root mean squared errors) vary from 0.016 to 0.022 of the normalized radius for storms lasting 2–3 days, with somewhat larger uncertainty observed for the lifetimes

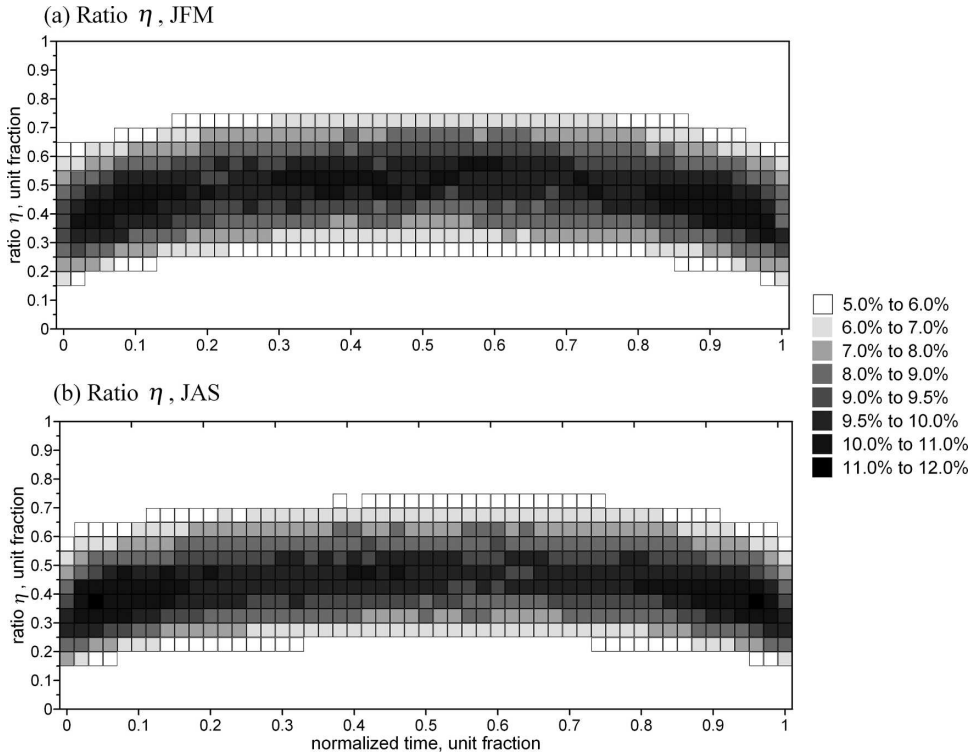

FIG. 11. (a) Winter and (b) summer evolution of the PDF of the ratio η, defining the cyclone asymmetry, during the nondimensional cyclone lifetime.

longer than 4–5 days for which the uncertainties of the approximation increase to 0.038.

Besides the changes in the cyclone effective radius, cyclones experience shape changes during their lifetime. Figure 11 shows the evolution of the ratio η during the nondimensional cyclone lifetime in the same manner as Fig. 9 does for the cyclone effective radius. During winter at the stage of the cyclone generation, η varies from 0.1 to 0.7 with a modal value of 0.38, implying quite a strong asymmetry in the cyclone shape. At the stage of the maximum cyclone intensity, the winter ratio of η approaches values of 0.3–0.8 and then decreases to values of 0.2–0.6 at the end of cyclone life cycle. During summer, values of η are 15%–20% smaller than in winter, implying stronger cyclone asymmetry in comparison to the winter months. The smallest modal values during summer are 0.35 with the largest being from 0.45 to 0.5. Thus, seasonal changes in the ratio η vary by 20%–25%. The most intense cyclones demonstrate larger values of η, being more symmetric during the cyclone life cycle. For the cyclones with a minimum central pressure less than 980 hPa, the ratio between the smallest and the largest radii grows from 0.5 to 0.65 from cyclone generation to the stage of the maximum cyclone intensity and then decreases to 0.4 at the stage of the cyclone decay (not shown).

6. Summary and discussion

We analyzed a climatology of cyclone size characteristics and their change during the cyclone life cycle in the Northern Hemisphere. For this purpose we used a cylindrical coordinate transform and established a unique reference coordinate system for the further interpolation of SLP and the analysis of cyclone geometry. This methodology was applied to the results of a numerical cyclone tracking algorithm, using SLP data from the NCEP–NCAR reanalysis for the period 1948–2004. Climatological estimates of the cyclone effective radius are statistically significantly larger over the oceans than over the continents, which are characterized by the presence of small nonbaroclinic transients. Analysis of the cyclone size evolution during cyclone life cycle shows growing cyclone size during the cyclone development and decreasing of the cyclone radius during decay. Changes in radius during the cyclone life cycle typically vary from 100 km for short-lived cyclones to about 400 km for the cyclones with a lifetime longer than 5 days. The behavior of the cyclone size during development implies a universal relationship between the normalized cyclone radius and normalized lifetime. This allowed for the development of a parameterization of the cyclone size change during the cy-

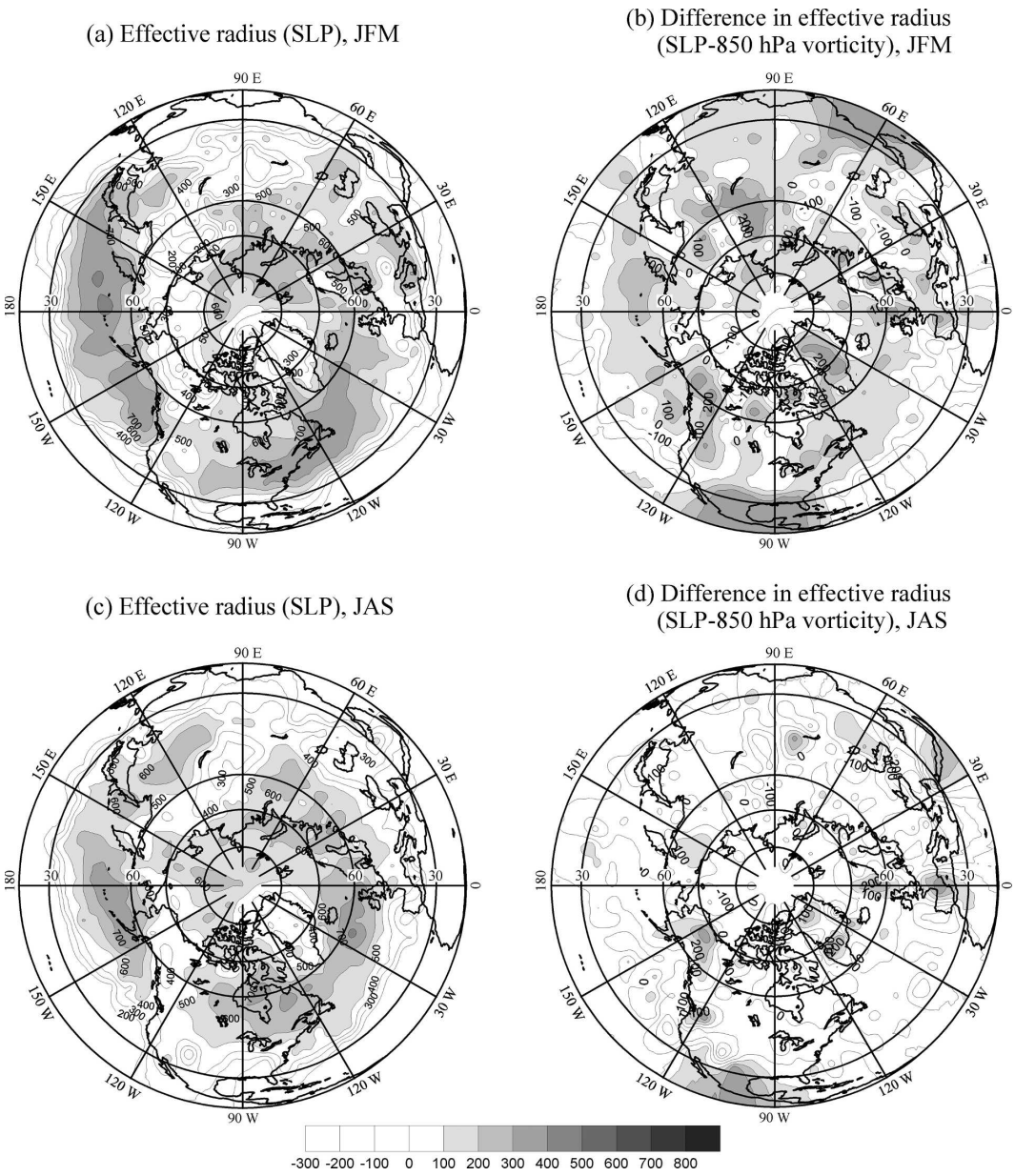

FIG. 12. (a) Winter and (c) summer climatological distribution of the cyclone effective radius (km) derived from the SLP-based tracking for the cyclones living longer than 2 days, and (b) winter and (d) summer differences between the cyclone effective radius derived SLP-based and vorticity-based tracking (km). Contour interval is 100 km.

clone life cycle. The parameterization also accounts for the cyclone intensity and is applicable for cyclone lifetimes from 18 h to 7 days.

Our results can be discussed from a number of view points. In contrast to similar methodology used by Simmonds (2000) and Simmonds and Keay (2000a) our estimates of cyclone radii are somewhat larger, a difference that can be explained by some differences in the search procedures. Simmonds and Keay (2000a) defined the edge of the cyclone at the location where the Laplacian vanishes, while in our work the edge is identified as the location where the azimuthal pressure gradient falls to zero. This difference may imply that larger radii are calculated using our methodology. Another important question is the extent to which the choice of cyclone tracking algorithm may influence the results. To test the sensitivity of cyclone size estimates to the tracking scheme used, we performed the tracking of the

vorticity at 850 hPa as recommended by Hoskins and Hodges (2002) and Hodges et al. (2003). For the analysis we applied a cutoff of cyclones that live less than 2 days, as was done in the works of Sinclair (1997) and Hodges et al. (2003). The distribution of the annual mean number of cyclones is qualitatively very similar in both tracking outputs, which is consistent with Hodges et al. (2003) (not shown). However, in contrast to Hodges et al. (2003), the vorticity-based tracking shows a 5%–15% increase in the number of cyclones over the oceans and somewhat smaller counts over the continents. For instance, the Mediterranean storm track is much better represented in the SLP tracking. We have to note, however, that Hodges et al. (2003) analyzed results for the winter period only.

The climatology of cyclone effective radius estimated from the SLP-based tracking after the application of the cutoff of short-lived cyclones (Figs. 12 a,b) shows 10%–15% larger values than those obtained using all cyclones living longer than 18 h (Fig. 3). Figures 12c,d show that the SLP-based tracking compared with the vorticity-based gives approximately 50–100 km larger estimates in winter for and up to 100 km smaller values in summer over most oceanic and continental storm tracks. Over mountain regions, SLP-based tracking implies systematically larger cyclone sizes that should be considered in the context of the reliability of SLP fields in these areas. However, both methodologies imply significant changes in the cyclone size during the cyclone life cycle. To the extent that it is possible to draw physical inferences with the present level of uncertainty, we can conclude that cyclone size grows during the cyclone development stage by 50%–150% over the Northern Hemisphere for all seasons with the largest growth observed for the most intense events over oceanic storm tracks. This estimate of cyclone size change is somewhat larger than that reported by Simmonds (2000) and closer to the estimates given by Grotjahn et al. (1999). However, Simmonds (2000) considered mean cyclone radii, while we take into account the asymmetry of the distributions of cyclone sizes at the stages of their early development and decay.

We selected from our archive the 12 storms analyzed by Grotjahn et al. (1999) and estimated changes in cyclone effective radius for this subset. Figure 13 shows the dependence of the relative growth of cyclone effective radius (as adopted here) versus the duration of the cyclone development stage. The results imply that the cyclones grow from 20% to about 300% during their development stage with a mean estimate of about 80%. This qualitatively is consistent with Grotjahn et al. (1999), although there are cyclones that exhibit larger and smaller growth than the implied by their study.

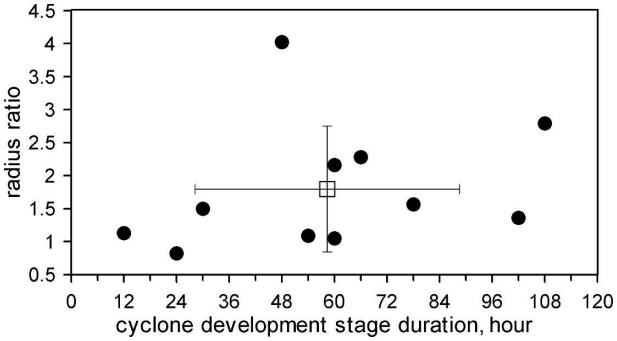

FIG. 13. Dependence of the relative growth of the cyclone effective radius on the cyclone development stage duration for the Pacific cyclones analyzed by Grotjahn et al. (1999). The open square shows the average over 12 estimates. Horizontal and vertical bars correspond to standard deviations of the cyclone development stage duration and the growth of the cyclone effective radius.

Grotjahn et al. (1999) reasonably argue that their results might be sensitive to the choice of the basic wavelet functions used for the analysis. Moreover, Grotjahn et al. (1999) initially used the data truncated to T42 spectral resolution. Blender and Schubert (2000) and recently Jung et al. (2006) have shown that the truncation may significantly affect the results of the tracking. Since the cyclones typically develop in a nonuniform background SLP field, which was not removed in this study, it is difficult to distinguish between the contribution of background field effects and nonlinear mechanisms (Grotjahn 1996) in cyclone size changes. Martin and Otkin (2004) used the fifth-generation Pennsylvania State University–NCAR Mesoscale Model to analyze the changes of potential vorticity due to the diabatic sources of latent heat in a rapidly intensifying Pacific cyclone and demonstrated noticeable changes of the cyclone geometry. Grotjahn et al. (2003) in a model study argued that nonlinear mechanisms may be responsible for the evolution of horizontal sizes of the synoptic eddies. Mechanisms in the upper troposphere that may be responsible for the cyclone geometry change were considered by Nielsen-Gammon and Lefevre (1996).

In this respect it is interesting to identify the cyclones that do not change size during their development. We selected transients whose effective radius undergoes no significant changes during the life cycle by applying a threshold of $\pm 10\%$ change in the effective radius. Altogether we found 230 cyclones during 57-yr period; that is, less than 1% of the total number of cyclones, with the most such events during spring and autumn (about 170 cyclones). Figure 14a shows the spaghetti plot of the tracks of all cyclones that do not experience significant changes in size during the cyclone life cycle.

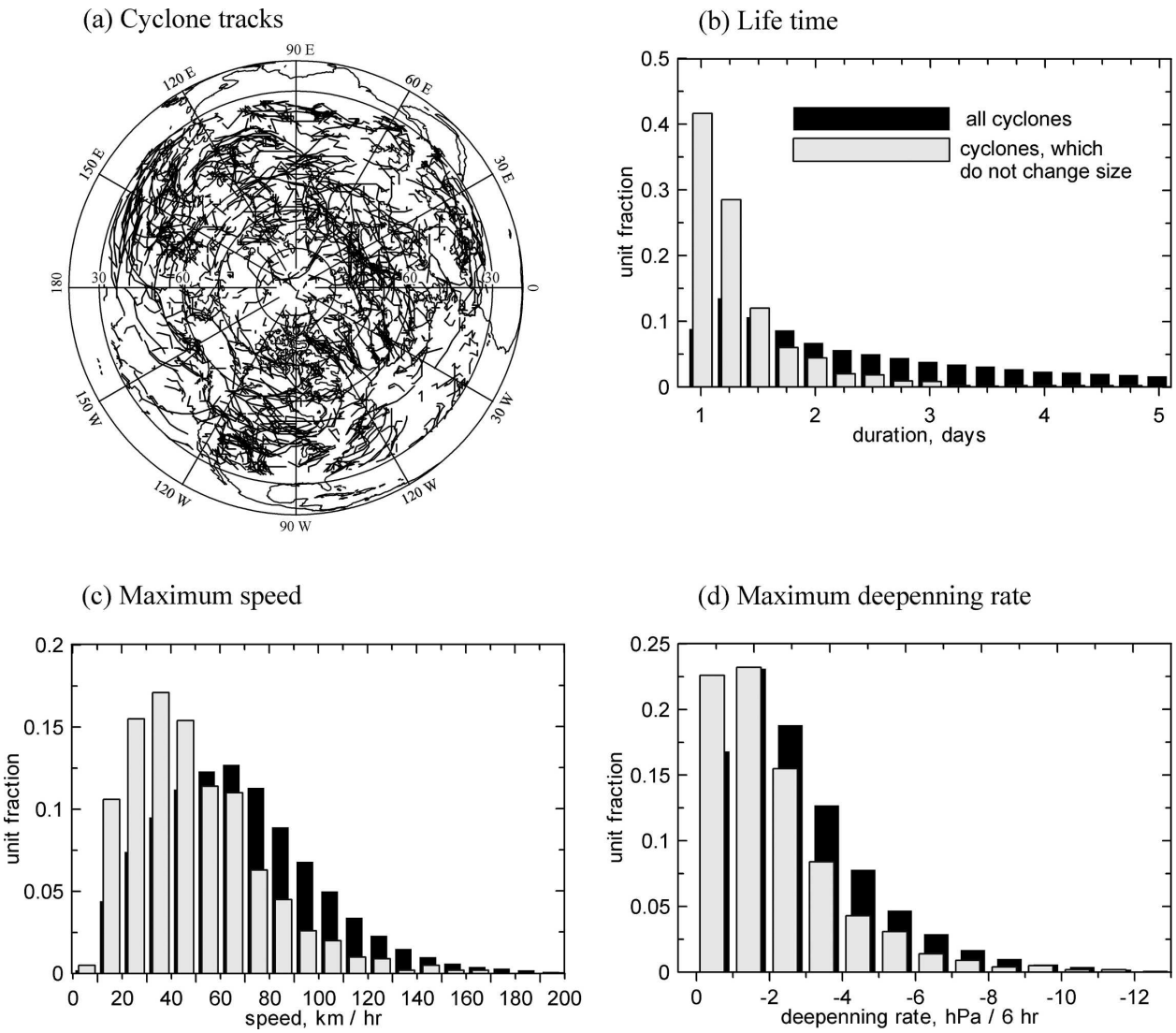

FIG. 14. Trajectories of the cyclones which do not experience significant change in size during the lifetime for (a) the period 1948–2004, (b) occurrence histograms of the cyclone lifetime, (c) cyclone maximum propagation velocity, and (d) cyclone deepening rate for all cyclones (black) and cyclones that do not indicate changes in size (white).

The density of these tracks is somewhat higher over the continents than over the oceans. Most of these cyclones are characterized by a track length of 200 to 2000 km while a typical cyclone track is several times longer. Figure 14b shows that cyclones that do not change size are characterized by a considerably shorter lifetime. The threshold of 2 days on cyclone lifetime (Sinclair 1997; Hodges et al. 2003) eliminates practically all these cyclones. The maximum cyclone propagation velocity (Fig. 14c) for these cyclones implies modal values of 20–50 km h^{-1} (45% of cyclones), 25–30 km h^{-1} smaller than the typical maximum propagation velocity. The maximum deepening rates (Fig. 14d) for these cyclones are considerably smaller than for full set of trajectories. It is very likely that the uncommon cyclones of unchanging size may result from the difficulties and uncertainties of storm tracking and cyclone geometry estimation (both of which increase for short-lived and stationary systems).

Of interest is the dependency of the number of simultaneously existing cyclones over the globe on their sizes (Golitsyn et al. 2007), which can be also derived from our estimates. Generally, an increasing number of gyres implies smaller individual sizes if the globe geometry and rotation are not changed. We derived cyclone counts (with no regard to storm intensity and age) simultaneously identified over the hemisphere at every 6-hourly step and estimated their mean effective radius

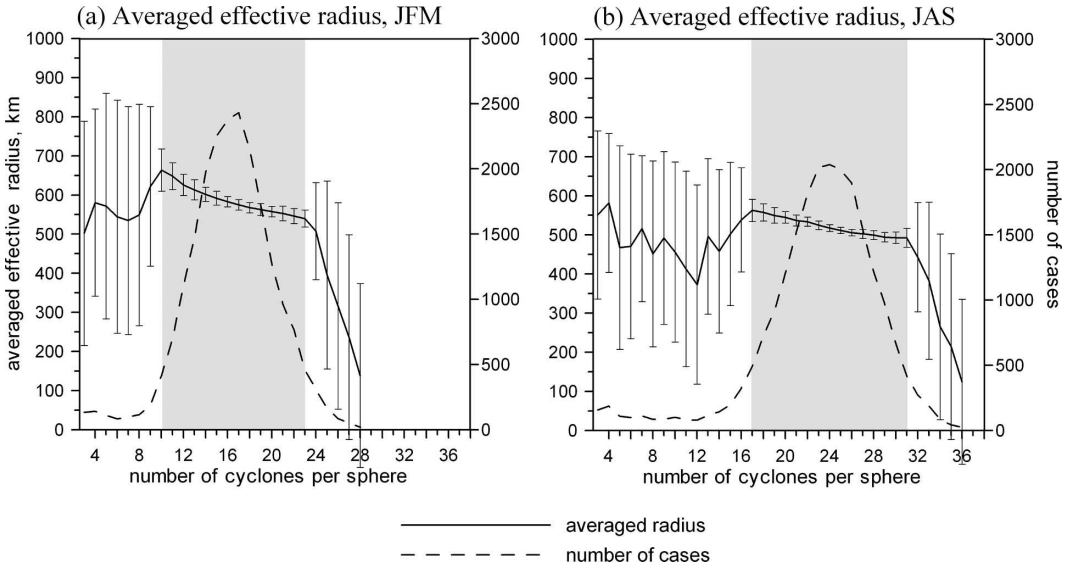

FIG. 15. Cyclone effective radius averaged for different numbers of cyclones (solid lines), simultaneously existing over the Northern Hemisphere, along with the number of cases (dashed lines) with given number of simultaneously existing transients for (a) winter and (b) summer seasons.

for 1948–2004. Figure 15 shows the dependency of the mean cyclone radius on the number of cyclones along with the number of cases used. The number of transients simultaneously identified over the Northern Hemisphere varies from less than 5 to more than 30 with the typical number ranging between 10 and 25 in winter and between 17 and 33 in summer. Mean cyclone effective radius is clearly larger for cases of small cyclone numbers (>650 km in winter and >550 km in summer) and decreases by approximately 100–150 km for cases when more than 20 cyclones simultaneously exist over the Northern Hemisphere.

There are several lines of development for further application of our results. The methodology allows for the effective construction of cyclone composites for different geographical areas or different stages of cyclone development (Lackmann et al. 1996; Yoshida and Asuma 2004; Bauer and Del Genio 2006). Cyclone composites may be very effective for analysis of the cyclone energy balance and the role of different mechanisms in the cyclone water and energy cycles. Ruprecht et al. (2002) analyzed composites of cyclones in the eastern Atlantic for the estimation of the water vapor transport by atmospheric synoptic transients. However, they used a simplified procedure for averaging the fields within the same 10° box for the time periods when cyclone center was identified as approximately in the center of the box. The analyses of the cyclone size and shape changes made during storm tracking may significantly improve the accuracy of the identification of storms. Particularly, analysis of the radial pressure gradients may help to identify multicenter depressions and to distinguish between them and propagating cyclones. Of particular interest is the analysis of climate variability in cyclone size and shape, which we will perform in the future. This will allow for the association of the major circulation modes with changes in cyclone size and will help to identify the circulation regimes responsible for the occurrence of cyclones with different geometry.

Acknowledgments. We thank our colleagues Olga Zolina and Vladimir Soloviov of IORAS (Moscow), Georgy Golitsyn of IAP (Moscow), Thomas Jung of ECMWF (Reading), and Eberhard Ruprecht of IFM-GEOMAR (Kiel) for the useful discussions on different aspects of this work. Great thanks to Helmut Haak of MPI (Hamburg) and Jean-Marc Molines of LEGI (Grenoble) who provided us with the technical advice on the coordinate transformation. We highly appreciate the suggestions and criticism of Ron McTaggart-Cowan and the three anonymous reviewers, which were extremely helpful for the improvement of the first version of the manuscript. This work was supported by Russian Foundation for Basic Research (Grant 05-05-64506), Russian Ministry of Education and Science under the Federal "World Ocean" Programme, and by the NATO SfP Project 981044.

REFERENCES

Akima, H., 1970: A new method of interpolation and smooth curve fitting based on local procedures. *J. ACM,* **17,** 589–602.

Bauer, M., and A. D. Del Genio, 2006: Composite analysis of winter cyclones in a GCM: Influence on climatological humidity. *J. Climate,* **19,** 1652–1672.

Bengtsson, L., K. I. Hodges, and S. Hagemann, 2004: Sensitivity of the ERA-40 reanalysis to the observing system: Determination of the global atmospheric circulation from reduced observations. *Tellus,* **56A,** 456–471.

——, ——, and E. Roeckner, 2006: Storm tracks and climate change. *J. Climate,* **19,** 3518–3543.

Blender, R., and M. Schubert, 2000: Cyclone tracking in different spatial and temporal resolutions. *Mon. Wea. Rev.,* **128,** 377–384.

——, K. Fraedrich, and F. Lunkeit, 1997: Identification of cyclone track regimes in the North Atlantic. *Quart. J. Roy. Meteor. Soc.,* **123,** 727–741.

Geng, Q., and M. Sugi, 2001: Variability of the North Atlantic cyclone activity in winter analyzed from NCEP–NCAR reanalysis data. *J. Climate,* **14,** 3863–3873.

Golitsyn, G. S., I. I. Mokhov, M. G. Akperov, and M. Yu. Bardin, 2007: Distribution functions of probabilities of cyclones and anticyclones from 1952 to 2000: An instrument for the determination of global climate variations. *Dokl. Earth Sci.,* **413,** 324–326.

Grigoriev, S., S. Gulev, and O. Zolina, 2000: Innovative software facilitates cyclone tracking and analysis. *Eos, Trans. Amer. Geophys. Union,* **81,** 170.

Grotjahn, R., 1996: Vorticity equation terms for extratropical cyclones. *Mon. Wea. Rev.,* **124,** 2843–2858.

——, and C. Castello, 2000: A study of frontal cyclone surface and 300-hPa geostrophic kinetic energy distribution and scale change. *Mon. Wea. Rev.,* **128,** 2865–2874.

——, D. Hodyss, and C. Castello, 1999: Do frontal cyclones change size? Observed widths of North Pacific lows. *Mon. Wea. Rev.,* **127,** 1089–1095.

——, ——, and S. Immel, 2003: A technique for creating linearly stable localized atmospheric features with an application to nonlinear cyclogenesis. *Dyn. Atmos. Oceans,* **37,** 25–54.

Gulev, S. K., O. Zolina, and S. Grigoriev, 2001: Extratropical cyclone variability in the Northern Hemisphere winter from the NCEP/NCAR reanalysis data. *Climate Dyn.,* **17,** 795–809.

——, T. Jung, and E. Ruprecht, 2002: Climatology and interannual variability in the intensity of synoptic-scale processes in the North Atlantic from the NCEP–NCAR reanalysis data. *J. Climate,* **15,** 809–828.

Hines, K. M., D. H. Bromwich, and G. J. Marshall, 2000: Artificial surface pressure trends in the NCEP–NCAR reanalysis over the Southern Ocean and Antarctica. *J. Climate,* **13,** 3940–3952.

Hodges, K. I., 1994: A general method for tracking analysis and its application to meteorological data. *Mon. Wea. Rev.,* **122,** 2573–2586.

——, 1999: Adaptive constraints for feature tracking. *Mon. Wea. Rev.,* **127,** 1362–1373.

——, B. J. Hoskins, J. Boyle, and C. Thorncroft, 2003: A comparison of recent reanalysis datasets using objective feature tracking: Storm tracks and tropical easterly waves. *Mon. Wea. Rev.,* **131,** 2012–2037.

Hoskins, B. J., and K. I. Hodges, 2002: New perspectives on the Northern Hemisphere winter storm tracks. *J. Atmos. Sci.,* **59,** 1041–1061.

——, and ——, 2005: A new perspective on Southern Hemisphere storm tracks. *J. Climate,* **18,** 4108–4129.

Humphreys, W. J., 1927: The greater increase in size and intensity of the extratropical cyclone by night than by day. *Mon. Wea. Rev.,* **55,** 496.

Jung, T., S. K. Gulev, I. Rudeva, and V. Soloviov, 2006: Sensitivity of extratropical cyclone characteristics to horizontal resolution in the ECMWF model. *Quart. J. Roy. Meteor. Soc.,* **132,** 1839–1857.

Kalnay, E., and Coauthors, 1996: The NCEP/NCAR 40-Year Reanalysis Project. *Bull. Amer. Meteor. Soc.,* **77,** 437–471.

Kistler, R., and Coauthors, 2001: The NCEP–NCAR 50-Year Reanalysis: Monthly means CD-ROM and documentation. *Bull. Amer. Meteor. Soc.,* **82,** 247–267.

König, W. R., R. Sausen, and F. Sielmann, 1993: Objective identification of cyclones in GCM simulations. *J. Climate,* **6,** 2217–2231.

Lackmann, G. M., L. F. Bosart, and D. Keyser, 1996: Planetary- and synoptic-scale characteristics of explosive wintertime cyclogenesis over the western North Atlantic Ocean. *Mon. Wea. Rev.,* **124,** 2672–2702.

Lim, E.-P., and I. Simmonds, 2002: Explosive cyclone development in the Southern Hemisphere and a comparison with Northern Hemisphere events. *Mon. Wea. Rev.,* **130,** 2188–2209.

Martin, J. E., and J. A. Otkin, 2004: The rapid growth and decay of an extratropical cyclone over the central Pacific Ocean. *Wea. Forecasting,* **19,** 358–376.

Murray, R. J., and I. Simmonds, 1991: A numerical scheme for tracking cyclone centres from digital data. Part I: Development and operation of the scheme. *Aust. Meteor. Mag.,* **39,** 155–166.

Nielsen, J. W., and R. M. Dole, 1992: A survey of extratropical cyclone characteristics during GALE. *Mon. Wea. Rev.,* **120,** 1156–1167.

——, and R. J. Lefevre, 1996: Piecewise tendency diagnosis of dynamical processes governing the development of an upper-tropospheric mobile trough. *J. Atmos. Sci.,* **53,** 3120–3142.

Roebber, P. J., 1984: Statistical analysis and updated climatology of explosive cyclones. *Mon. Wea. Rev.,* **112,** 1577–1589.

——, 1989: On the statistical analysis of cyclone deepening rates. *Mon. Wea. Rev.,* **117,** 2293–2298.

Rogers, E., and L. F. Bosart, 1986: An investigation of explosively deepening oceanic cyclones. *Mon. Wea. Rev.,* **114,** 702–718.

Ruprecht, E., S. S. Schroeder, and S. Ubl, 2002: The North Atlantic Oscillation and the water transport over Europe. *Meteor. Z.,* **11,** 395–401.

Sanders, F., and J. R. Gyakum, 1980: Synoptic-dynamic climatology of the "bomb." *Mon. Wea. Rev.,* **108,** 1589–1606.

Serreze, M. C., 1995: Climatological aspects of cyclone development and decay in the Arctic. *Atmos.–Ocean,* **33,** 1–23.

——, F. Carse, R. G. Barry, and J. C. Rogers, 1997: Icelandic low cyclone activity: Climatological features, linkages with the NAO, and relationships with recent changes in the northern hemisphere circulation. *J. Climate,* **10,** 453–464.

Sickmöller, M., R. Blender, and K. Fraedrich, 2000: Observed winter cyclone tracks in the northern hemisphere in reanalysed ECMWF data. *Quart. J. Roy. Meteor. Soc.,* **126,** 591–620.

Simmonds, I., 2000: Size changes over the life of sea level cyclones in the NCEP reanalysis. *Mon. Wea. Rev.,* **128,** 4118–4125.

——, and R. J. Murray, 1999: Southern extratropical cyclone behavior in ECMWF analyses during the FROST special observing periods. *Wea. Forecasting,* **14,** 878–891.

——, and K. Keay, 2000a: Mean Southern Hemisphere extratrop-

ical cyclone behavior in the 40-year NCEP–NCAR reanalysis. *J. Climate,* **13,** 873–885.
——, and ——, 2000b: Variability of Southern Hemisphere extratropical cyclone behavior, 1958–97. *J. Climate,* **13,** 550–561.
——, and ——, 2002: Surface fluxes of momentum and mechanical energy over the North Pacific and North Atlantic Oceans. *Meteor. Atmos. Phys.,* **80,** 1–18.
Sinclair, M. R., 1994: An objective cyclone climatology for the Southern Hemisphere. *Mon. Wea. Rev.,* **122,** 2239–2256.
——, 1997: Objective identification of cyclones and their circulation, intensity and climatology. *Wea. Forecasting,* **12,** 591–608.
——, and I. G. Watterson, 1999: Objective assessment of extratropical weather systems in simulated climates. *J. Climate,* **12,** 3467–3485.
Trigo, I. F., 2006: Climatology and interannual variability of storm-tracks in the Euro-Atlantic sector: A comparison between ERA-40 and NCEP/NCAR reanalyses. *Climate Dyn.,* **26,** 127–143.
White, G., 2000: Long-term trends in the NCEP/NCAR reanalysis. *Proc. Second Int. Conf. on Reanalyses,* Reading, United Kingdom, ECMWF, WCRP-109, WMO Tech. Doc. 985, 54–57.
Yoshida, A., and Y. Asuma, 2004: Structures and environment of explosively developing extratropical cyclones in the northwestern Pacific region. *Mon. Wea. Rev.,* **132,** 1121–1142.
Zolina, O., and S. K. Gulev, 2002: Improving the accuracy of mapping cyclone numbers and frequencies. *Mon. Wea. Rev.,* **130,** 748–759.
——, and ——, 2003: Synoptic variability of ocean–atmosphere turbulent fluxes associated with atmospheric cyclones. *J. Climate,* **16,** 2717–2734.